Low-field spin dynamics of Cr_7Ni and Cr_7Ni-Cu-Cr_7Ni molecular rings as detected by μSR

S. Sanna,[1] P. Arosio,[2,*] L. Bordonali,[3] F. Adelnia,[2] M. Mariani,[3] E. Garlatti,[4] C. Baines,[5] A. Amato,[5] K. P. V. Sabareesh,[3,6] G. Timco,[7] R. E. P. Winpenny,[7] S. J. Blundell,[8] and A. Lascialfari[2]

[1]*Department of Physics and Astronomy, University of Bologna, 40127 Bologna, Italy*
[2]*Dipartimento di Fisica, Università degli studi di Milano, and INSTM, I-20133 Milano, Italy*
[3]*Department of Physics, Università degli studi di Pavia-CNISM, I-27100 Pavia, Italy*
[4]*Dipartimento di Scienze Matematiche, Fisiche e Informatiche, Università di Parma, I-43124 Parma, Italy*
[5]*Paul Scherrer Institute, CH-5232 Villigen, Switzerland*
[6]*University of Information Science and Technology "St. Paul the Apostle", 6000 Ohrid, R. Macedonia*
[7]*The Lewis Magnetism Laboratory, School of Chemistry, The University of Manchester, Manchester M13 9PL, United Kingdom*
[8]*Department of Physics, Oxford University, Oxford OX1 3PU, United Kingdom*

(Received 17 July 2017; revised manuscript received 12 October 2017; published 3 November 2017)

Muon spin rotation measurements were used to investigate the spin dynamics of heterometallic Cr_7Ni and Cr_7Ni-Cu-Cr_7Ni molecular clusters. In Cr_7Ni the magnetic ions are arranged in a quasiplanar ring and interact via an antiferromagnetic exchange coupling constant J, while Cr_7Ni-Cu-Cr_7Ni is composed of two Cr_7Ni linked by a bridging moiety containing one Cu ion, that induces an inter-ring ferromagnetic interaction $J' \ll J$. The longitudinal muon relaxation rate λ collected at low magnetic fields $\mu_0 H < 0.15$ Tesla, shows that the two systems present differences in spin dynamics vs temperature. While both samples exhibit a main peak in the muon relaxation rate vs temperature, at $T \sim 10$ K for Cr_7Ni and $T \sim 8$ K for Cr_7Ni-Cu-Cr_7Ni, the two compounds have distinct additional features: Cr_7Ni shows a shoulder in $\lambda(T)$ for $T < 8$ K, while Cr_7Ni-Cu-Cr_7Ni shows a flattening of $\lambda(T)$ for $T < 2$ K down to temperatures as low as $T = 20$ mK. The main peak of both systems is explained by a Bloembergen-Purcell-Pound (BPP)-like heuristic fitting model that takes into account of a distribution of electronic spin characteristic times for $T > 5$ K, while the shoulder presented by Cr_7Ni can be reproduced by a BPP function that incorporates a single electronic characteristic time theoretically predicted to dominate for $T < 5$ K. The flattening of $\lambda(T)$ in Cr_7Ni-Cu-Cr_7Ni occurring at very low temperature can be tentatively attributed to field-dependent quantum effects and/or to an inelastic term in the spectral density of the electronic spin fluctuations.

DOI: 10.1103/PhysRevB.96.184403

I. INTRODUCTION

It was the late 1980s when molecular magnets started to receive a progressively increasing attention due to their possible applications in several fields, the first recognized to be memory storage [1]. Since then, their potential uses have been extended to the fields of quantum information processing (QIP) [2] and, more recently, spintronics [3]. Particularly, in the last ten years suitable systems for QIP were identified in antiferromagnetic (AFM) heterometallic wheels [4], a particular class of molecules composed of a finite number of transition-metal ions arranged in a planar or quasiplanar regular ring. In all molecular magnets, each molecule is magnetically quasi-isolated from the others, thus allowing to study the single unit properties by investigating a bulk system. In AFM wheels, inside the single molecule each ion is coupled with its neighbor via a strong antiferromagnetic exchange interaction J and, depending on the magnitude of J and of the different intramolecular anisotropies, the electronic dominating characteristic time could become long enough to allow for instance QIP, the main limitation being the very low temperature where this occurs. As a consequence, the experimental investigation of the magnetic properties and, particularly, of the spin dynamics of AFM rings is relevant for a complete understanding of the mechanisms affecting quantum coherence and decoherence. Muon spin rotation (μSR), nuclear magnetic resonance (NMR), and electron spin resonance (ESR) are excellent choices for probing the local dynamics and have been proved useful in understanding the static and dynamic magnetic properties of a significant number of molecular magnets [5–15]. Particularly μSR has the advantage to use very low or zero applied magnetic field, a situation where in most cases the zero-field energy levels and the magnetic dynamics of the system are slightly perturbed.

A specific example of molecular magnet possibly useful for applications where the typical characteristic times are important, is given by the so-called Cr_7Ni AFM ring [2,16,18], whose magnetic core consists of seven $s = 3/2$ Cr^{3+} ions and one $s = 1$ Ni^{2+} ion (which breaks the spin lattice symmetry) forming an octagonal planar ring. The total ground-state spin of the Cr_7Ni molecule is $S_T = 1/2$, resulting from the AFM couplings Cr^{3+}-Ni^{2+} and Cr^{3+}-Cr^{3+} among the magnetic ions. The Cr_7Ni system has been demonstrated to have long coherence time $T_2 \approx 3$ μs at $T < 5$ K by pulsed ESR echo experiments [17], which can be improved dramatically by chemically engineering the molecular structure to optimize the environment of the spin [18]. Relaxation dynamics in this system is driven by spin-phonon interactions, as it has been confirmed by ^{1}H-NMR nuclear spin-lattice (longitudinal) relaxation rate $1/T_1$ measurements [19]. On the other hand Timco *et al.* [2] demonstrated that when two Cr_7Ni molecules are joined together by a metallic Cu^{2+}-based linker, the resulting Cr_7Ni-Cu-Cr_7Ni system exhibits quantum spin

*paolo.arosio@unimi.it

entanglement at low temperature emerging from the magnetic coupling of the two spin-1/2 Cr_7Ni rings with the spin-1/2 of the Cu^{2+} ion, an occurrence suggesting that this system can be used to implement quantum gates.

^{1}H-NMR measurements of $1/T_1$ vs temperature showed that for magnetic fields chosen in the range $0.47 < \mu_0 H < 1.7$ Tesla, Cr_7Ni and Cr_7Ni-Cu-Cr_7Ni (in short Cr_7Ni-ent) have the same spin dynamics at intermediate temperatures $T > 5$–10K, while down to temperatures as low as 80 mK the data are inconclusive [20], although the presence of spin freezing is demonstrated.

In this paper, we present a μSR investigation of the heterometallic Cr_7Ni and Cr_7Ni-ent rings in longitudinal field, aimed at highlighting the difference in the spin dynamics among the two systems at low magnetic fields, possibly caused by the intermolecular coupling occurring via the Cu bridge in Cr_7Ni-ent. In fact, the longitudinal muon relaxation rate λ behavior as a function of temperature at constant low magnetic fields $\mu_0 H < 0.15$ Tesla, presents some differences in the two systems. At intermediate temperature $5 < T < 60$ K, we show that both samples present a main peak of $\lambda(T)$ at constant H occurring at $T \sim 10 \pm 1$K for Cr_7Ni and $T \sim 8 \pm 1$K for Cr_7Ni-ent, but Cr_7Ni shows also a shoulder in $\lambda(T)$ for $T < 8$ K. The main peak of both systems is explained in terms of a heuristic Bloembergen-Purcell-Pound (BPP)-like fitting model that takes into account a distribution of electronic spin characteristic times for $T > 5$ K (see also Ref. [20] for a comparison with NMR data). The shoulder presented by Cr_7Ni can be reproduced by a BPP function containing a single electronic characteristic time as theoretically predicted by Bianchi *et al.* [19]. On the other hand, in the Cr_7Ni-ent compound $\lambda(T)$ for $T < 2$ K flattens to a value that decreases by increasing the field. This flattening could possibly have quantum origin or could originate from inelastic terms contributing to λ.

II. EXPERIMENTAL DETAILS

Two polycrystalline samples of antiferromagnetic heterometallic rings have been prepared following Refs. [2,16]; their structures are shown in Fig. 1. In the first sample, $[Me_2H_2Cr_7NiF_8(OCCMe_3)_{16}]$ (in short Cr_7Ni), the magnetic core is composed by a single ring of seven Cr^{3+}, $s = 3/2$, ions and one Ni^{2+}, $s = 1$, ion interacting via two slightly different exchange antiferromagnetic (AF) coupling constants Cr-Cr ($J_{\text{Cr-Cr}}/k_B$) and Cr-Ni ($J_{\text{Cr-Ni}}/k_B$). Thus, the resulting AF ground state has total spin $S_T = 1/2$, with $J_{\text{Cr-Cr}}/k_B \sim 16.9$ K and $J_{\text{Cr-Ni}}/k_B \sim 19.6$ K [22]. The second sample, namely $[NH_2Pr_2]\,[Cr_7NiF_8(O_2CCMe_3)_{15}(O_2CC_5H_4N)]_2$ [Cu(NO3)2(OH2)] (in short Cr_7Ni-ent), is composed of two single Cr_7Ni rings interacting through an organic bridge including a Cu^{2+} ion, thereby giving rise to the phenomenon of quantum entanglement, as previously remarked. Theoretical calculation, specific heat, and EPR characterization measurements [2,21] indicates that this Cu bridge promotes a weak additional ferromagnetic exchange interaction coupling, $J' \sim 1$ K, which entangles the respective single-molecule wave functions at the first excited state.

To have magnetic data for μSR analysis, dc magnetization measurements have been performed by a commercial superconducting quantum interferometer device (SQUID) MPMS-XL7 by Quantum Design. All collected data resulted in agreement with previous results [2,19]. Field-cooled (FC) measurements of magnetic susceptibility $\chi(T) \simeq M/H$ have been performed on Cr_7Ni and Cr_7Ni-ent powders, in the temperature range $2 < T < 300$ K under an applied dc field $\mu_0 H = 0.1$ Tesla (Fig. 2, main graph). M vs H curves have been collected at $T = 2K$ on both systems in the range $0 - 7$ Tesla (Fig. 2, insets).

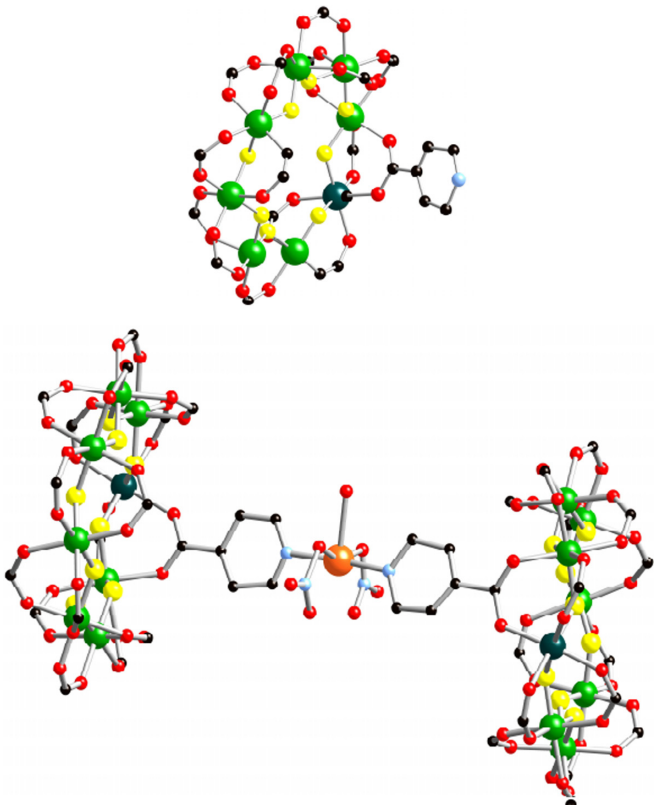

FIG. 1. Structure of the single molecule of Cr_7Ni (top) and Cr_7Ni-ent (bottom). Light green: Cr; dark green: Ni, F; yellow: O; red: C; black, light blue: N.

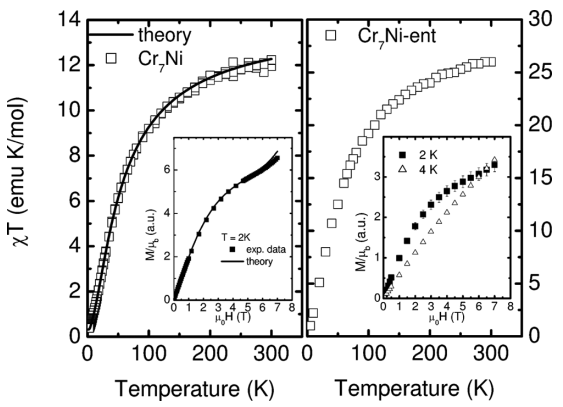

FIG. 2. Temperature evolution of $\chi \cdot T$ of Cr_7Ni (left) and Cr_7Ni-ent (right) in an applied magnetic field $\mu_0 H = 0.1$ Tesla in field cooling conditions. Insets: magnetic moment as a function of the magnetic field (for Cr_7Ni-ent at two different temperatures).

Positive muon spin relaxation (μSR) measurements were performed on samples in powder, in longitudinal (i.e., parallel to the muon beam) applied magnetic fields (LF) fields $\mu_0 H =$ 80, 148 mTesla for Cr_7Ni in the temperature range $1.5 < T <$ 70 K, and in LF fields $\mu_0 H = 20$, 60, 80, 148 mTesla for Cr_7Ni-ent, in the temperature range $0.02 < T < 70$ K. Experiments were run at the continuous muon source of the Paul Scherrer Institute with the GPS (for 1.6 K $< T <$ 200 K) and LTF (for temperatures down to 20 mK) spectrometers. In μSR, 100%-spin-polarized positive muons directed antiparallel to the beam momentum are implanted in the sample, and the time-dependent response of the $s = 1/2$ muon spin interaction with the local magnetic environment is monitored via the positrons emitted by millions of muon decay events. From the collection of the emitted positrons, it is possible to extract the muon asymmetry $A(t) = [N_F(t) - N_B(t)]/[N_F(t) + N_B(t)]$, $N_{F/B}$ being the sum of the decay positrons recorded by a set of counters placed forward/backward to the sample with respect to the initial polarization of the muon beam. This time-differential signal is proportional to the muon spin or depolarization function $G^{\mu}(t)$, which results from static or quasistatic (for example, the spatial disorder present in the local magnetic field) and dynamic (such as local field fluctuations) processes.

III. RESULTS AND DISCUSSION

The magnetic behavior shows an antiferromagnetic ground state for both Cr_7Ni and Cr_7Ni-ent samples (Fig. 2). The results are in good agreement with previous studies [2,16].

The Cr_7Ni-ent supramolecular compound can be described by the following spin Hamiltonian:

$$H = H_{\text{ring}}(1) + H_{\text{ring}}(2) + H_{\text{Cu}} + H_{\text{int}}(1) + H_{\text{int}}(2), \quad (1)$$

where the subsystems 1 and 2 correspond to the two Cr_7Ni rings described by the Hamiltonians H_{ring}, H_{Cu} is the single Cu ion linker term and H_{int} accounts for the ring-linker interactions.

The Hamiltonian for each Cr_7Ni molecule can be written as

$$\begin{aligned} H_{\text{ring}} = & \sum_{i=1}^{N} J_i \mathbf{s}_i \cdot \mathbf{s}_{i+1} + \sum_{i=1}^{N} d_i s_{z,i}^2 \\ & + \sum_{i>j=1}^{N} D_{ij}[2s_{z,i}s_{z,j} - s_{x,i}s_{x,j} - s_{y,i}s_{y,j}] \\ & - \mu_{\text{B}} \sum_{i=1}^{N} g_i \mathbf{B} \cdot \mathbf{s}_i, \end{aligned} \quad (2)$$

where $s = 3/2$ for Cr^{3+}, $s = 1$ for Ni^{2+}, and $N = 8$ is the number of magnetic ions in the molecule, with the usual cyclic boundary condition $N + 1 = 1$, assuming Ni on site 8. The first term in Eq. (2) corresponds to the dominant antiferromagnetic isotropic exchange interaction. The second term describes the axial single-ion zero-field-splitting terms (with $d_{\text{Cr}} = -0.35$ K, $d_{\text{Ni}} = -4$ K and the z axis perpendicular to the ring) [22], while the third term is the axial contribution to the dipolar anisotropic intracluster spin-spin interaction, where D_{ij} is evaluated within the point-dipole approximation.

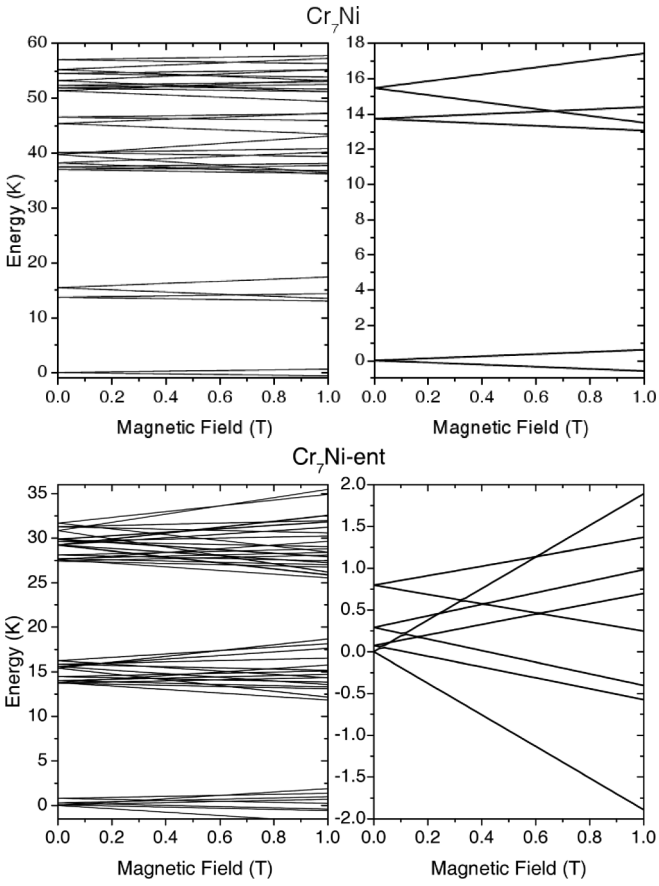

FIG. 3. Magnetic field dependence of the energy levels of Cr_7Ni (top) and Cr_7Ni-ent (bottom) calculated with Eqs. (1)–(4). Left side: full structure of the energy levels. Right side: zoom on the lowest levels. The magnetic field is applied along the z axis, perpendicular to the planes of the rings.

The last term represents the Zeeman coupling with an external field $\mathbf{H}$ (with $g_{\text{Cr}} = 1.98$ and $g_{\text{Ni}} = 2.2$).

The linker consists of a single Cu^{2+} ion:

$$H_{\text{Cu}} = -\mu_{\text{B}} \mathbf{B} \cdot \mathbf{g}_{\text{Cu}} \cdot \mathbf{s}_{\text{Cu}} \quad (3)$$

(with $\mathbf{g}_{\text{Cu}}$ as in Ref. [2]), and the Hamiltonian describing the coupling between each ring and the linker is

$$H_{\text{int}} = J' \mathbf{s}_{\text{Cu}} \cdot [\mathbf{s}_{Cr} + \mathbf{s}_{Ni}], \quad (4)$$

where $J' = -1$ K and $\mathbf{s}_{Cr}$ and $\mathbf{s}_{Ni}$ correspond to $\mathbf{s}_1$ and $\mathbf{s}_8$ in their respective rings.

The calculated magnetic field dependence of the energy levels of Cr_7Ni and Cr_7Ni-ent are reported in Fig. 3. Following the Hamiltonian in Eq. (2), in zero applied magnetic field, the energy levels structure of Cr_7Ni features a doubly degenerate $S_T = 1/2$ ground state, separated by an energy gap $\Delta E \simeq$ 13.7 K from the first excited state, an $S_T = 3/2$ state. On the other hand, Cr_7Ni-ent displays a more complex configuration of the lowest levels: due to the magnetic coupling between the two Cr_7Ni units and the Cu^{2+} ion, the magnetic ground state of the molecule has a total spin $S_T = 3/2$ state split by the zero-field splitting anisotropy into two doublets, $|3/2, \pm 3/2\rangle$ and $|3/2, \pm 1/2\rangle$. Two additional $S_T = 1/2$ excited states are separated by energies within 1 K from the ground state and

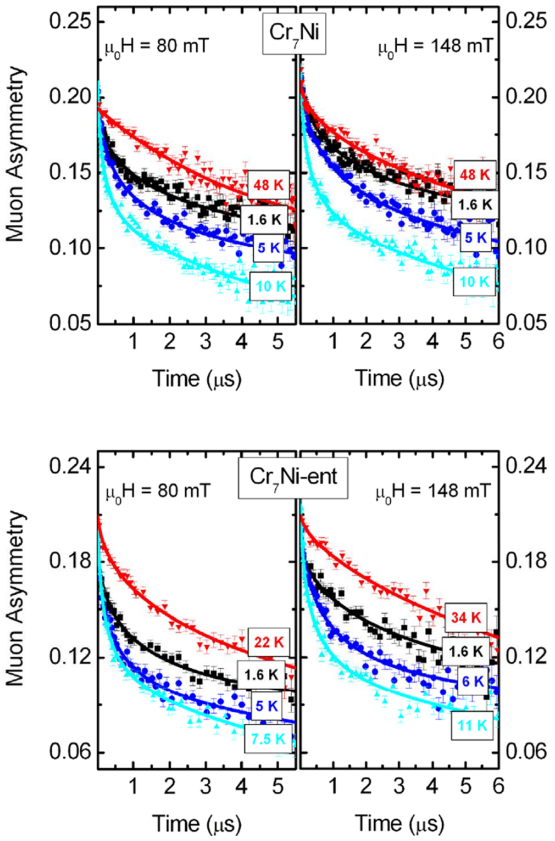

FIG. 4. Time evolution of the μSR asymmetry for the Cr_7Ni (top) and Cr_7Ni-ent (bottom) samples at representative temperatures with a longitudinal applied field $\mu_0 H = 80$ and 148 mT (left and right panels respectively). The solid line is the best fit to Eq. (5).

spin entanglement effects in Cr_7Ni-ent can be observed on this small energy scale [2].

The time evolution of the μSR asymmetry is displayed in Fig. 4 for some representative temperatures with longitudinal applied fields $\mu_0 H = 80$ and 148 mTesla. As in previous μSR studies of nanomagnets [10,11], a single exponential term does not adequately account for the relaxation, and the best fitting of the total relaxing asymmetry requires the following function:

$$A(t) = a_f \exp(\lambda_f t)^{1/2} + a_s \exp(\lambda_s t) + a_{bg}, \tag{5}$$

where $a_f = 0.1(0.005)$ and $a_s = 0.11(0.005)$ are the amplitudes of two relaxing components and λ_f and λ_s their corresponding relaxation rates; $a_{bg} = 0$ for GPS beam line and $a_{bg} = 0.02$ for LTF, is a background component. The first term in Eq. (5) is a root exponential with a faster decay rate ($\lambda_f \sim 1$–$4 \mu s^{-1}$), which reflects a broad distribution of couplings of the muon to the magnetic moment, due to the multiplicity of possible muon stopping sites in each molecule implanted around the magnetic ions. The second term with a slower decay rate ($\lambda_s \sim 0.1$–$1\ \mu s^{-1}$) indicates the presence of a muon site farther away from the magnetic molecular core. For the rest of the paper we will focus on the slow rate $\lambda_s(T,H) \equiv \lambda(T,H)$; it is worth to remark that the behavior of λ_f vs T and H is very similar to the one of λ_s.

The temperature behavior of the longitudinal muon relaxation rate $\lambda(T)$ probes the phonon-induced molecular spin relaxation dynamics [23–25] that causes the muon spin depolarization. In fact, by considering the hyperfine muon-electron (muon-molecular) interaction as a perturbation, one can use the so-called weak-collision theory where, starting from the general Hamiltonian of the electron-muon system, the longitudinal relaxation rate can be written as [8,9]:

$$\lambda \propto k_B T \sum_{ij} \beta_{ij} J_z^{ij}(\omega_L), \tag{6}$$

where i,j number the electronic spins, ω_L is the Larmor frequency of the muon spin, β_{ij} is a hyperfine factor, and J_z^{ij} is the longitudinal spectral density of the electronic (molecular) spin fluctuations [8,9]. The wave vector q dependence of $J_z^{ij}(\omega_L)$ was neglected due to the relatively high temperature and to the presence of a set of inequivalent (crystallographically and from the point of view of hyperfine interactions) muons. The spectral density J_z^{ij} can be expressed by the Fourier transform (FT) of the spin-spin correlation function $G_z^{ij}(t)$:

$$J_z^{ij}(\omega_L) = \int G_z^{ij}(t) e^{i\omega_L t} dt. \tag{7}$$

Limiting to the case $i = j$ (autocorrelation) one can find that the function $J_z(\omega_L)$ [$\equiv J_z^{ii}(\omega_L)$], i.e., the spectrum of fluctuations of the longitudinal magnetization M_z of the molecule at ω_L, depends on several relaxation rates connected to the specific relaxation path of M_z, so that [25]:

$$J^z(\omega_L,T,H) = \sum_{i=1,n} A(\Gamma_i,T,H) \frac{\Gamma_i(T,H)}{\omega_L^2 + \Gamma_i(T,H)^2}, \tag{8}$$

where $\mu_0 H$ is the external magnetic field and $1/\Gamma_i = \tau_i$ are different characteristic correlation times of the magnetization fluctuations.

It should now be remarked that, in several μSR and NMR cases [8] concerning molecular nanomagnets where a single characteristic time τ_c is dominating, the muon spin-lattice relaxation rate λ ($\equiv 1/T_1$ of NMR case) vs temperature at different applied magnetic fields follows the universal Bloembergen-Purcell-Pound (BPP) law [23–25]:

$$\lambda = K \chi T \frac{\tau_c}{1 + \omega_L^2 \tau_c^2}, \tag{9}$$

where K is a hyperfine constant. The thermal fluctuations of the electronic molecular spins generate fluctuations of the local fields at the muon site. Indeed, the characteristic time τ_c in Eq. (9) is related to the phonon-induced decay of the electronic spins fluctuations, which in this case takes place through one single dominating process. Thus, the spectral density $J(\omega_L)$ reduces to a single Lorenztian of width τ_c. τ_c is generally temperature dependent and it may follow, according to different theoretical frameworks, a power law [23,24] or a thermally activated behavior described by the Arrhenius law [25]. A peak of $\lambda/(\chi T)$ is observed when $1/\tau_c = \omega_L(H)$, i.e., when the frequency of the electronic spin fluctuations equals the Larmor frequency. Hence, as a consequence of Eq. (9), the height of the peaks measured with different fields scales as $1/H$ following the BPP behavior.

Contrarily to this simple scenario, in Ref. [19] it has been shown that Cr_7Ni doesn't follow the BPP behavior, since, even in a single τ_c regime, the presence of inequivalent ions prevents

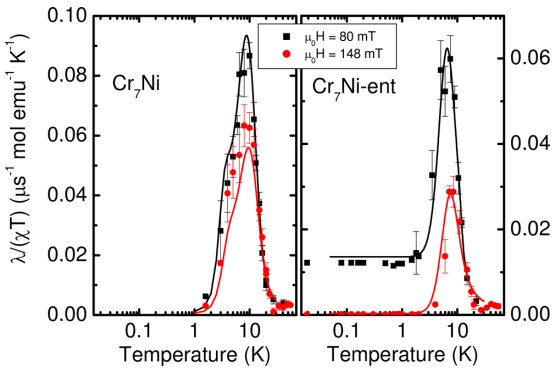

FIG. 5. Temperature dependence of $\lambda_s/(\chi T)$ for both the Cr_7Ni (left) and Cr_7Ni-ent (right) samples in longitudinal applied field $\mu_0 H = 80$ and 148 mT. The solid lines are the best fit to Eq. (10) and (12) for Cr_7Ni (left) and Cr_7Ni-ent respectively.

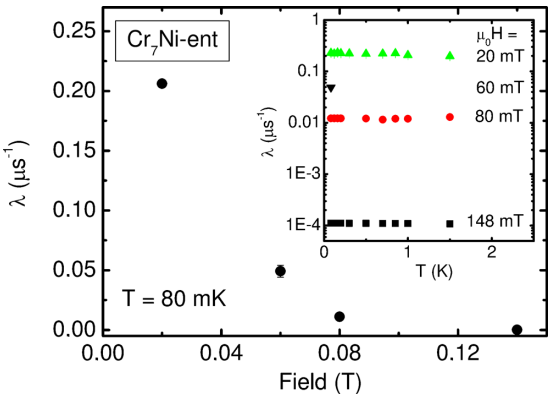

FIG. 6. Relaxation rate λ_s from the muon asymmetry fitting by Eq. (5) for Cr_7Ni-ent as a function of the longitudinal applied field $\mu_0 H$. Inset: temperature dependence of λ_s for different applied fields in the regime of very low temperatures.

mapping local-spin correlations with the corresponding total-spin ones. Thus, λ and $1/T_1$ are no longer proportional to $J^z(\omega_L, T, H)$, but are a linear combination of the spectral densities of the single-ion magnetic moments, and $A(\Gamma_i, T, H)$ is not proportional to χT. Moreover, it has been demonstrated that when several relaxation channels are contributing to the relaxation dynamics, not only Cr_7Ni but also homometallic molecular nanomagnets do not follow the BPP behavior [19,26,27].

Figure 5 displays the behavior of $\lambda/(\chi T)$ as a function of temperature for both Cr_7Ni and Cr_7Ni-ent at the two different applied fields $\mu_0 H = 80$ and 148 mTesla. Both samples display a peaked behavior around 10 K for all the applied fields, in qualitative agreement with previous NMR measurements on Cr_7Ni [19]. Cr_7Ni displays also a shoulder in $\lambda(T)$ for $T < 8$ K while Cr_7Ni-ent for $\mu_0 H = 80$ mTesla and $T < 2$ K clearly shows a flattening to a nonzero λ value down to 80 mK. This flattening, observed also in other molecular clusters [6,15], indicates the presence of a residual spin-lattice relaxation channel down to the lowest temperature. This effect has been studied as a function of the field and will be discussed below. The formula of Eq. (9) with a single dominant characteristic time τ_c failed to reproduce the experimental data for both samples and, consequently, we used more complex expressions presented here below.

For the Cr_7Ni compound, a sum of two BPP-like terms is required to fit the experimental data:

$$\frac{\lambda}{\chi T} = K_1 \frac{\tau_{c1}}{1+\omega_0^2\tau_{c1}^2} + K_2 \int_0^\infty \frac{f(E)\tau_{c2}(E)}{1+\omega_0^2\tau_{c2}^2(E)}\, dE \qquad (10)$$

with $\tau_{ci}(E) = \tau_{0i} e^{E_i/kT}$, $i = 1,2$, and

$$f(E) = \frac{1}{\sqrt{2\pi}\sigma} \exp\left[-\frac{(E-\mu)^2}{2\sigma^2}\right]. \qquad (11)$$

The first term fits the shoulder shown by $\lambda/(\chi T)$ data at low temperatures ($T \sim 3$ K, Fig. 5, left) and yields $\tau_{01} = 33 \pm 9$ ns and $E_1/k_B = 12.0 \pm 3.2$ K, in agreement with previous calculations [19] that predicted a single dominating characteristic time for temperatures $T < 5$ K. It should be noted that the theoretical calculations of the characteristic times entering the spectral density reported in Ref. [19] have been performed at a different magnetic field ($\mu_0 H = 400$ mTesla) with respect to the one used in the current experiments ($\mu_0 H = 80$ mTesla). The second term fits the data for $T > 5$ K and reproduces the muon peak occurring at $T \simeq 10$ K, by assuming a distribution of characteristic times, which leads to a distribution of energy barriers E, described for simplicity with a Gaussian distribution represented in Eq. (11). The fit results yield $\tau_{02} = 0.65 \pm 0.14$ ns and an average energy barrier $E_2/k_B = 58.6 \pm 4.1$ K with a distribution width $\sigma = 22.1 \pm 5.1$ K. The presence of the Gaussian distribution in the second term of Eq. (7), necessary to fit the main λ peak, reflects the existence of more than one phonon-induced relaxation channel, in the region $T > 5$–8 K (in agreement with theory [19]).

As concerns the data fitting of Cr_7Ni-ent compound the following function is required:

$$\frac{\lambda}{\chi T} = \text{const.} \times [1 - \tanh(T)] + K_3 \int_0^\infty \frac{f(E)\tau_{c3}(E)}{1+\omega_0^2\tau_{c3}^2(E)}\, dE, \qquad (12)$$

where the first term mimics the flattening at low T and the second term is similar to the second contribution to λ in Eq. (10). The fit yields $\tau_{03} = 4.1 \pm 0.3$ ns and an average energy barrier $E_3/k_B = 34.3 \pm 0.8$ K with a width $\sigma = 11.2 \pm 0.3$ K. Also in the case of Cr_7Ni-ent, the presence of the second term in Eq. (12) is due to a distribution of electronic characteristic times.

In order to go into deeper details of the very low temperature ($T \leqslant 1.5$ K) spin dynamics of Cr_7Ni-ent we investigated the field dependence of the muon longitudinal relaxation rate as a function of the LF at constant low temperature, where the flattening of λ does occur (inset in Fig. 6). The main panel of Fig. 6 shows at $T = 80$ mK a fast reduction of λ as a function of the field in the range 20–148 mTesla here investigated. This $\lambda(H)$ behavior at constant T persists until $T = 1.5$ K, as can be evinced from the inset of Fig. 6, where λ appears constant in the range 20 mK $< T \leqslant 1.5$ K for all applied magnetic fields. In particular, for $\mu_0 H = 148$ mTesla the value of λ is very near to zero, i.e., the muon polarization does not relax anymore.

The flattening of λ vs T at constant applied LF was already observed in other molecular magnets [10–13,15] at zero or low applied fields. Though this phenomenon could possibly have a quantum origin, it has to be noticed that also inelastic terms in the spectral density $J(\omega)$ contributing to λ can give similar effects [28]. In any event, a relaxation channel still active at these extremely low temperatures has to be found and the explanation of the experimental data remains a matter of debate.

IV. CONCLUSIONS

We have investigated the molecular magnetic ring Cr_7Ni vs the Cr_7Ni-ent system constituted by two Cr_7Ni units interacting via a Cu(II)-based bridging moiety, with the aim of investigating the spin dynamics at low magnetic fields by μ^{SR}. We showed that the muon longitudinal relaxation rate λ behavior, as a function of temperature and field displays a main peak at intermediate temperatures of the order of 10 K for both systems (see also Ref. [20] for higher field NMR data), explained by assuming a distribution of characteristic times related to more than one electronic transition and phonon-induced relaxation paths. For $T < 5$ K, the Cr_7Ni compound reveals a dynamic behavior guided by a single characteristic time, as evinced by a shoulder present in $\lambda(T)$. On the other hand, until extremely low temperature $T \sim 20$ mK, $\lambda(T)$ for Cr7Ni-ent flattens to a value, which is field dependent. The physical origin of this flattening has still to be understood although, due to very low temperature and the independence on T, one could guess an active channel of relaxation of quantum origin and/or a contribution to λ coming from inelastic terms in the spectral density of the electronic spin fluctuations.

ACKNOWLEDGMENTS

The projects EU-FP6-NoE MAGMANET and the FIRB Project No. RBFR12RPD1 of the Italian Ministry of Education and Research, are acknowledged for funding. We thank also S. Ferretti for help in experimental SQUID data collection and S. Carretta for giving the calculated theoretical curves $M(T)$ and $M(H)$ for Cr_7Ni. We thank Paul Scherrer Institut for giving access to the muon beam line.

[1] D. Gatteschi, R. Sessoli, and J. Villain, *Molecular Nanomagnets* (Oxford University Press, Oxford, 2006).

[2] G. A. Timco, S. Carretta, F. Troiani, F. Tuna, R. J. Pritchard, C. A. Muryn, E. J. L. McInnes, A. Ghirri, Andrea Candini, P. Santini, G. Amoretti, Marco Affronte, and R. E. P. Winpenny, Nat. Nanotechnol. **4**, 173 (2009).

[3] L. Bogani and W. Wernsdorfer, Nat. Mater. **7**, 179 (2008); M. Mannini, F. Pineider, P. Sainctavit, C. Danieli, E. Otero, C. Sciancalepore, A. M. Talarico, M.-A. Arrio, A. Cornia, D. Gatteschi, and R. Sessoli, *ibid.* **8**, 194 (2009).

[4] A. Candini, G. Lorusso, F. Troiani, A. Ghirri, S. Carretta, P. Santini, G. Amoretti, C. Muryn, F. Tuna, G. Timco, E. J. L. McInnes, R. E. P. Winpenny, W. Wernsdorfer, and M. Affronte, Phys. Rev. Lett. **104**, 037203 (2010); S. Gao, *Molecular Nanomagnets and Related Phenomena*, 2nd ed. (Springer, Berlin, 2015).

[5] A. Lascialfari, Z. H. Jang, F. Borsa, P. Carretta, and E. D. Gatteschi, Phys. Rev. Lett. **81**, 3773 (1998).

[6] Z. Salman, A. Keren, P. Mendels, V. Marvaud, A. Scuiller, M. Verdaguer, J. S. Lord, and C. Baines, Phys. Rev. B **65**, 132403 (2002).

[7] S. J. Blundell, F. L. Pratt, T. Lancaster, I. M. Marshall, C. A. Steer, W. Hayes, T. Sugano, J.-F. Letard, A. Caneschi, D. Gatteschi, and S. L. Heath, Physica B **326**, 556 (2003).

[8] F. Borsa, A. Lascialfari, and Y. Furukawa, in *Novel NMR and EPR Techniques*, edited by J. Dolinsek, M. Vilfan, and S. Zumer, NMR in Magnetic Molecular Rings and Clusters (Springer, Berlin, 2006), pp. 297–349.

[9] C. P. Slichter, *Principles of Magnetic Resonance*, 2nd ed. (Springer-Verlag, Berlin, 1996).

[10] D. Procissi, A. Lascialfari, E. Micotti, M. Bertassi, P. Carretta, Y. Furukawa, and P. Kogerler, Phys. Rev. B **73**, 184417 (2006).

[11] J. Lago, E. Micotti, M. Corti, A. Lascialfari, A. Bianchi, S. Carretta, P. Santini, D. Procissi, S. H. Baek, P. Kogerler, C. Baines, and A. Amato, Phys. Rev. B **76**, 064432 (2007).

[12] S. J. Blundell, Contemp. Phys. **48**, 275 (2007).

[13] T. Lancaster, J. S. Möller, S. J. Blundell, F. L. Pratt, P. J. Baker, T. Guidi, G. A. Timco, and R. E. P. Winpenny, J. Phys.: Condens. Matter **23**, 242201 (2011).

[14] T. Lancaster, S. J. Blundell, F. L. Pratt, I. Franke, A. J. Steele, P. J. Baker, Z. Salman, C. Baines, I. Watanabe, S. Carretta, G. A. Timco, and R. E. P. Winpenny, Phys. Rev. B **81**, 140409(R) (2010).

[15] A. Keren, O. Shafir, E. Shimshoni, V. Marvaud, A. Bachschmidt, and J. Long, Phys. Rev. Lett. **98**, 257204 (2007).

[16] F. K. Larsen, E. J. L. McInnes, H. El Mkami, J. Overgaard, S. Piligkos, G. Rajaraman, E. Rentschler, A. A. Smith, G. M. Smith, V. Boote, M. Jennings, G. A. Timco, and R. E. P. Winpenny, A. Chem, Int. Ed. **42**, 101 (2003).

[17] A. Ardavan, O. Rival, J. J. L. Morton, S. J. Blundell, A. M. Tyryshkin, G. A. Timco, and R. E. P. Winpenny, Phys. Rev. Lett. **98**, 057201 (2007).

[18] C. J. Wedge, G. A. Timco, E. T. Spielberg, R. E. George, F. Tuna, S. Rigby, E. J. L. McInnes, R. E. P. Winpenny, S. J. Blundell, and A. Ardavan, Phys. Rev. Lett. **108**, 107204 (2012).

[19] A. Bianchi, S. Carretta, P. Santini, G. Amoretti, J. Lago, M. Corti, A. Lascialfari, P. Arosio, G. Timco, and R. E. P. Winpenny, Phys. Rev. B **82**, 134403 (2010).

[20] L. Bordonali, Y. Furukawa, M. Mariani, K. P. V. Sabareesh, E. Garlatti, S. Carretta, A. Lascialfari, G. Timco, R. E. P. Winpenny, and F. Borsa, J. Appl. Phys. **115**, 17E102 (2014).

[21] F. Troiani, M. Affronte, S. Carretta, P. Santini, and G. Amoretti, Phys. Rev. Lett. **94**, 190501 (2005).

[22] R. Caciuffo, T. Guidi, G. Amoretti, S. Carretta, P. Santini, C. Mondelli, G. Timco, C. A. Muryn, and R. E. P. Winpenny, Phys. Rev. B **71**, 174407 (2005).

[23] S. H. Baek, M. Luban, A. Lascialfari, E. Micotti, Y. Furukawa, F. Borsa, J. van Slageren, and A. Cornia, Phys. Rev. B **70**, 134434 (2004).

[24] I. Rousochatzakis, A. Lauchli, F. Borsa, and M. Luban, Phys. Rev. B **79**, 064421 (2009).

[25] P. Santini, S. Carretta, E. Liviotti, G. Amoretti, P. Carretta, M. Filibian, A. Lascialfari, and E. Micotti, Phys. Rev. Lett. **94**, 077203 (2005).

[26] E. Garlatti, S. Carretta, P. Santini, G. Amoretti, M. Mariani, A. Lascialfari, S. Sanna, K. Mason, J. Chang, P. Tasker, and E. K. Brechin, Phys. Rev. B **87**, 054409 (2013).

[27] E. Garlatti, S. Bordignon, S. Carretta, G. Allodi, G. Amoretti, R. De Renzi, A. Lascialfari, Y. Furukawa, G. A. Timco, R. Woolfson, R. E. P. Winpenny, and P. Santini, Phys. Rev. B **93**, 024424 (2016).

[28] E. Micotti, A. Lascialfari, F. Borsa, M. H. Julien, C. Berthier, M. Horvatic, J. van Slageren, and D. Gatteschi, Phys. Rev. B **72**, 020405(R) (2005).